Available online at www.sciencedirect.com
SCIENCE DIRECT
International Journal of Multiphase Flow 32 (2006) 717–738
International Journal of Multiphase Flow
www.elsevier.com/locate/ijmulflow

The formation of a liquid bridge during the coalescence of drops

S.P. Decent *, G. Sharpe [1], A.J. Shaw, P.M. Suckling [2]

School of Mathematics, The University of Birmingham, Edgbaston, Birmingham B15 2TT, UK

Received 6 June 2005; received in revised form 7 February 2006

Abstract

This paper examines a mathematical model for the coalescence of two viscous liquid volumes in an inviscid gas or in a vacuum which removes the pressure singularity at the instant of impact inherent in the classical formulation of the continuum model. The very early stages of coalescence are examined in order to study the formation of the liquid bridge in two cases: (i) for two infinitely long, coalescing liquid cylinders; and (ii) for two coalescing spheres. Numerical solutions are computed for the velocity and pressure fields in the flow in both cases, and they confirm the removal of the pressure singularity. Also, the free-surface position at small times is determined.

Keywords: Coalescence; Viscous; Surface tension

1. Introduction

The coalescence of liquid volumes is an important mechanism in a wide variety of engineering and industrial applications such as the transport of dispersions of a liquid in a chemical technology (e.g. manufacturing of powder), lab-on-chip devices, ink-jet printing and spray painting (where the drops interact on and with a solid substrate), sintering, and jet cleaning of equipment in food processing. This type of fluid flow involves a topological transition in the flow domain. Here we concentrate on the early stages of coalescence, including the instant that the droplets first touch and the moments immediately after, and restrict the analysis to cases where the liquid is surrounded by an inviscid gas or vacuum. Droplet coalescence has been studied experimentally by Menchaca-Rocha et al. (2001), Beysens et al. (2002) and Pergamalis (2002). The earliest images taken after the volumes have joined show that they are connected by a small liquid bridge. These works have been backed up by some numerical computations (Lafaurie et al., 1994; Menchaca-Rocha et al., 2001; Pergamalis, 2002), which show good agreement with the available experimental data once the liquid bridge has formed. There are a number of theoretical studies that have investigated the coalescence of liquid drops using classical

* Corresponding author. Tel.: +44(0)121 414 7566; fax: +44(0)121 414 3389.
E-mail address: decentsp@for.mat.bham.ac.uk (S.P. Decent).
[1] Current address: School of Mechanical Engineering, University of Leeds, Leeds LS2 9JT, UK.
[2] Current address: Materia Nova, University of Mons, MONS-7000, Belgium.

0301-9322/$ - see front matter © 2006 Elsevier Ltd. All rights reserved.
doi:10.1016/j.ijmultiphaseflow.2006.02.005

fluid mechanics and a mixture of analytical and computational methods: Hopper (1984, 1990, 1992, 1993), Lafaurie et al. (1994), Richardson (1997), Eggers et al. (1999), Keller et al. (2000), Pergamalis (2002), Duchemin et al. (2003) and Billingham and King (2005). Such solutions also agree with experimental observations once the liquid bridge is formed, but are limited by an unphysical pressure singularity which occurs at the instant that the coalescence process starts and located at the point where the volumes first touch. The problem is complicated by the fact that experimental observations are extremely difficult at very small times after the initial impact. The presence of this pressure singularity in the classical model implies that the physics inherent in the classical formulation is not sufficient to describe the whole coalescence process. Therefore to include the moment of impact, a modified approach incorporating extra physics into the model must be required.

An approach that could provide the necessary physics to analyse droplet coalescence without singularities (including the moment of impact) is to use a coupled molecular dynamics and continuum mechanics approach. The microscopic model could be used to simulate the very early stages of coalescence and the continuum mechanics model would take over at later times, with the results of the molecular dynamics calculations providing the initial conditions for the classical fluid mechanics equations. This is effectively the philosophy used in most previous theoretical studies, where typically the macroscopic continuum model is used and calculations are started from a time when a smooth free-surface (the liquid bridge) has already formed between the two volumes. Koplik and Banavar (1994) has alternatively proposed that a "mesoscopic" model might be possible, in which a hybrid macroscopic (i.e. continuum) model is combined seamlessly with a microscopic (i.e. molecular) model. The key question which we address here is whether a macroscopic (i.e. continuum) model can be used instead to describe the whole process, including this liquid bridge formation; hence can this liquid bridge formation be instead considered as a macroscopic event? There is experimental evidence that the classical kinematic boundary condition breaks down under certain circumstances (Jeong and Moffatt, 1992). So perhaps this might be a route to removing this singularity?

One possibility for a purely continuum mechanics (macroscopic) approach which removes the singularity has been proposed by Shikhmurzaev (2000) (from now on labelled *I*). At the point where the liquid volumes first touch, there is a cusp in the free-surface. This model predicts that this cusp propagates away from the initial impact point, and the liquid–gas free-surface becomes smooth at a finite distance from the point of initial contact, at a finite time after impact. This occurs since the cusp is allowed to continuously and smoothly open out, forming a smooth free-surface in finite time. A key feature of this model is that surface tension is no longer fixed as a constant, but can vary along the free-surface. Also, fluid particles are allowed in the model to enter or leave the free-surface, as observed in Jeong and Moffatt (1992).

This model considers an internal liquid interface that is formed between the two coalescing volumes at impact, consisting of the liquid particles trapped between the two drops. As the cusp opens out and propagates away from the point of initial contact, this internal liquid–liquid interface is left behind the cusp, and connects the two liquid volumes as the initial stages of coalescence occurs. This is the beginning of the formation of the liquid bridge. The model describes fluid particles which travel from the liquid–gas free-surface, through the opening propagating cusp, and onto this internal liquid–liquid interface connecting the two liquid volumes. As the opening cusp propagates outwards, the area of this internal liquid–liquid surface increases. The model allows these liquid particles which pass from the free-surface onto the liquid–liquid interface to lose their surface properties in finite time. This means that the surface tension associated with these fluid particles relaxes in finite time, starting from the equilibrium value of the surface tension of the free-surface and finishing a short time later at zero surface tension. In other words, this model allows for these trapped particles to take a finite time to adjust from being surface particles to particles in the interior of the fluid. This process allows for the formation of a "surface tension relaxation tail" behind the propagating, opening cusp. The interior angle (measured through the liquid) between the opening propagating free-surface and the surface tension relaxation tail (contact angle) starts at 180° and changes to 90° in finite time, at which time a smooth free-surface is formed.

These events will occur very quickly, but the model allows them to occur over a finite time interval rather than instantaneously (see Fig. 1). Immediately after the moment of impact, a cusp forms in the free-surface located at the point of impact of the two volumes. It propagates away from the impact point and opens out under the action of surface tension, marking the line of intersection between the liquid–gas free-surface and the trapped internal liquid–liquid interface (Fig. 1(a)). We call this an "opening propagating cusp",

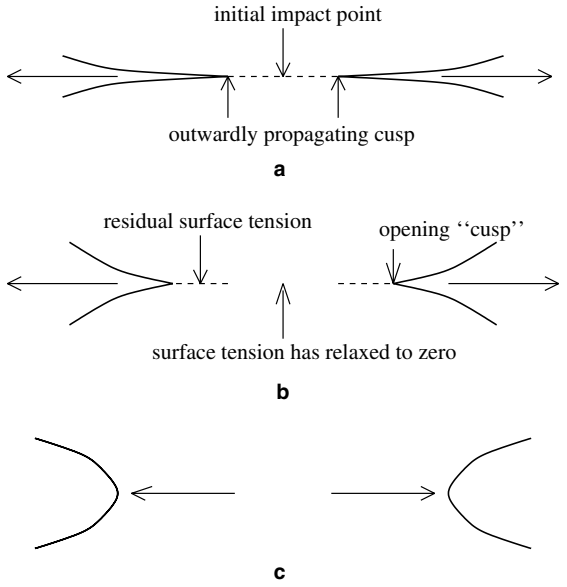

Fig. 1. A sketch of the early stages of coalescence.

though of course it is only a cusp initially when the interior contact angle is 180°. On the liquid–gas interface some distance away from this opening propagating cusp, the surface tension will be equal to the equilibrium value associated with the liquid–gas interface. Moving along the free-surface, towards the opening propagating cusp, surface tension will reduce smoothly. There is also some residual surface tension left along the trapped internal liquid–liquid interface and this smoothly reduces as one moves from the opening propagating cusp to the point of impact. As the opening cusp propagates away from the impact point, Fig. 1(b), the surface tension on the trapped internal liquid–liquid interface will reduce to zero (the equilibrium value associated with that interface). Here the surface tension relaxation tail is starting to disappear. The opening cusp will continue to propagate and will ultimately form a smooth free-surface, at which time the surface tension along all of the liquid–gas interface is at its equilibrium value and the surface tension along the whole of the interior liquid–liquid interface is zero (Fig. 1(c)). In Fig. 1, the trapped internal liquid–liquid interface is shown as the dashed horizontal line between the opening propagating cusps. Fluid particles travel from the free-surface onto this internal liquid–liquid interface as the cusp propagates outwards. On these dashed lines the surface tension is tending towards zero (the surface tension relaxation tail).

Like any new model, this theory of interface formation/disappearance requires testing, mathematically and experimentally, before it can be widely accepted (or if wrong, rejected). There is experimental evidence to support this model (Blake et al., 1999) but more work needs to be done to validate the model. We aim to critically test it in the case of coalescence by solving the model equations both asymptotically and computationally. This is particularly important, since if this model is correct, it would solve outstanding problems in (i) coalescence, (ii) jet breakup and film rupture (Shikhmurzaev, 2005a,b,c) and (iii) dynamic wetting (Shikhmurzaev, 1993, 1994, 1996, 1997, 2002). The interface formation model has, however, been criticised recently in Eggers and Evans (2004), though this criticism was rebutted by Shikhmurzaev and Blake (2004). Ultimately the interface formation model will either be accepted or rejected, like any theory, on the basis of comparison with experimental data. Thus in order to test whether this model is accurate and useful, it is necessary to compare computational and experimental results over the appropriate time interval, and this paper is a step towards producing the necessary numerical data.

The objectives of the research documented in this paper are: to test that this model has solutions of the type claimed in *I* in which the free-surface cusp centred at the point of coalescence propagates away from the point of impact and opens out; that the solutions are free of the pressure singularity inherent in the conventional approach; to suggest experimental regimes in which to test the theory. In *I* this theory was applied to the case of two coalescing liquid cylinders where a small time asymptotic approximation was derived. Here we extend

these asymptotics to determine the position of the free-surface at small times, and compute the velocity and pressure fields for the first time. Also, since coalescing cylinders are difficult to observe experimentally, these small time asymptotics are extended here to the case of two coalescing spheres for which numerical solutions are also computed.

2. Mathematical model

In the interface formation model (Shikhmurzaev, 1993–2005) the physical thicknesses of the internal liquid–liquid layer and the free-surface are assumed to be very small: estimates for simple fluids are of the order of nanometers (Blake et al., 1999; Blake and Shikhmurzaev, 2002; and *I*). For the purposes of the mathematical model the thickness of these interfaces is assumed to be infinitesimal and so they reduce to geometrical surfaces in the model.

The continuity and Navier–Stokes equations

$$\nabla \cdot \mathbf{u} = 0, \tag{1}$$

$$\frac{\partial \mathbf{u}}{\partial t} + (\mathbf{u} \cdot \nabla)\mathbf{u} = -\frac{1}{\rho}\nabla p + \nu \nabla^2 \mathbf{u} \tag{2}$$

are solved with a set of modified boundary conditions. Here t is time, $\mathbf{u}$ is the velocity of the liquid in the bulk, p is the bulk pressure, ρ is the density of the incompressible liquid and ν is the kinematic viscosity. The conventional viscous free-surface boundary conditions (on the liquid–gas interface) for constant surface tension are generalised to allow surface tension to vary and become

$$\frac{\partial G}{\partial t} + \mathbf{w} \cdot \nabla G = 0, \tag{3}$$

$$(\mathbf{I} - \mathbf{nn}) \cdot \mathbf{P} \cdot \mathbf{n} + \nabla \sigma = \mathbf{0}, \tag{4}$$

$$p_0 + \mathbf{n} \cdot \mathbf{P} \cdot \mathbf{n} = \sigma \nabla \cdot \mathbf{n}, \tag{5}$$

$$\sigma = \gamma(\varrho_0 - \varrho), \tag{6}$$

$$\frac{\partial \varrho}{\partial t} + \nabla \cdot (\varrho \mathbf{w}) = -\left(\frac{\varrho - \varrho_e}{\tau}\right), \tag{7}$$

$$(1 + 4\alpha\beta)\nabla\sigma = 4\beta(\mathbf{I} - \mathbf{nn}) \cdot (\mathbf{w} - \mathbf{u}) \tag{8}$$

and

$$\rho(\mathbf{u} - \mathbf{w}) \cdot \mathbf{n} = \frac{\varrho - \varrho_e}{\tau}. \tag{9}$$

These boundary conditions apply on the free-surface and also on the trapped interior liquid–liquid layer newly formed between the two liquid volumes (except for the normal stress boundary condition (5), which defines the free-surface position, and is only applied on the free-surface). Here $\mathbf{w}$ is the velocity with which the free-surface and the internal liquid–liquid interface are transported. Eq. (3) is the kinematic boundary condition for the free-surface $G(\mathbf{r}, t) = 0$, where $\mathbf{r}$ is the free-surface position vector. Eq. (4) is the tangential stress boundary condition where σ is the variable surface tension, $\mathbf{n}$ is the unit normal to the interface pointing into the liquid, $\mathbf{I}$ is the identity tensor, $\mathbf{P} = -p\mathbf{I} + \mu[\nabla\mathbf{u} + (\nabla\mathbf{u})^{\mathrm{T}}]$ is the stress tensor in the liquid, μ is viscosity and the superscript "T" denotes transpose. Note that Eq. (3) on the trapped internal liquid–liquid interface becomes $\mathbf{w} \cdot \mathbf{n} = 0$, since this internal interface will be assumed to be stationary.

Eq. (5) is the normal stress boundary condition where p_0 is the external pressure. The variation of surface tension is defined by the surface equation of state, Eq. (6), where γ is a liquid constant of linear proportionality and ϱ is the surface density associated with the interface (with dimensions of mass per unit area, since the interface is a geometrical surface of zero thickness in this model). The surface density that gives zero surface tension is ϱ_0 (this is required for equilibrium on the trapped interior liquid–liquid layer). Blake and Shikhmurzaev (2002) estimated that $\varrho_0 \approx \rho\delta l$ where δl is the thickness of the real physical interfacial layer. This thickness is likely to consist of several molecules and the liquid inside the interfacial layer is considered to be compressible. The interface mass conservation is quantified by the surface continuity Eq. (7). The term on the right-hand

side of Eq. (7) allows the surface density ϱ to relax to its equilibrium value ϱ_e in a finite time, and on the order of the surface tension relaxation time τ which will usually be very small (perhaps nano- or microseconds, and will have a characteristic value for any liquid at a given temperature). There are two parts to this interface: the trapped interior liquid–liquid interface and the liquid–gas free-surface. The surface tension on the liquid–liquid interface will eventually reach an equilibrium value of zero when the volumes have coalesced (this corresponds to the eventual disappearance of the surface tension relaxation tail). Surface tension along the liquid–gas free-surface will relax to some positive equilibrium value which corresponds to the equilibrium surface tension of that interface. Thus σ relaxes to its equilibrium along each interface in a time of order τ.

So far, values used for τ in the various studies are only estimates. Appropriate experiments will have to be designed (with the help of modelling such as described here and in the referenced works) to provide more precise measurements. In *I*, τ was estimated to range from 10^{-9} to 10^{-7} seconds for low to medium viscosity fluids. Davies and Rideal (1963) estimated that the surface tension relaxation time for water is of the order nanoseconds. In an experimental study carried out in Blake and Shikhmurzaev (2002), a series of water–glycerol liquids were considered where their viscosities ranged from 1.5×10^{-3} to 0.67 Pa s. For the least viscous liquids in that study, τ was estimated to be 10^{-9} to 10^{-8} s. For the most viscous liquids τ was estimated to be 10^{-6} to 10^{-5} s by comparing theoretical and experimental results. It was also hypothesised in Blake and Shikhmurzaev (2002) from experimental data that the surface tension relaxation time is proportional to the viscosity. Since there are commercially available silicone oils that have viscosities of the order of 10^3 Pa s, if $\tau\propto\mu$ one might expect silicone oils to have surface tension relaxation times of the order of milliseconds. This would make them suitable candidate fluids for experimental studies on liquid bridge formation because τ might then be sufficiently large for these events to be recorded by high speed photography. A much smaller estimate for τ of 10^{-18} s was given in Eggers and Evans (2004) (see Shikhmurzaev et al., 2004 for a comment on this estimate).

Let x be the distance from the point of initial contact through a line which passes through the propagating, opening cusp. Also let $x=x_*(t)$ be the location of the cusp. Then the equilibrium surface density ϱ_e is given by

$$\varrho_e=\begin{cases}\varrho_0, & 0\leqslant x<x_*(t),\\ \varrho_{1e}, & x>x_*(t),\end{cases} \tag{10}$$

where ϱ_{1e} is the equilibrium surface density at the liquid–gas free-surface and $\varrho_{1e}<\varrho_0$. Thus the equilibrium surface tension on the free-surface is $\sigma_{1e}=\gamma(\varrho_0-\varrho_{1e})$ and the equilibrium surface tension on the trapped interior liquid–liquid interface is zero. The dominant flow in the early stages of coalescence is driven by surface tension and the surface tension gradient is specified by boundary condition (8). Here α and β are constants that represent properties of the liquid (estimates for α and β are given in Blake and Shikhmurzaev, 2002). Eq. (9) specifies the mass transfer between the fluid bulk and the interfaces.

The surface parameters σ, ϱ, $\mathbf{w}$ are defined only on the interface, i.e. the "interface" is the trapped interior liquid–liquid interface between the two volumes as well as the free-surface at the liquid–gas interface. Since the publication of *I*, the interface formation/disappearance theory has been generalised to allow for a mass flux out of the interfacial layer (Shikhmurzaev, 2002, 2005a,b,c). Eqs. (9) and (8) replace Eqs. (18) and (17) in *I* respectively. It should be noted that the magnitude of the effects of this modification are of the order ϱ_e/ρ. Since ϱ_e is a surface density (mass in the surface divided by surface area), and ρ is a bulk density, then ϱ_e/ρ is of the order δl, the width of the interfacial layer. This will be approximately nanometres, or less, in most liquids and therefore it may be reasonable to expect that this mass transfer represented by the right-hand side of (9) is negligible. We shall discuss this point further in later sections.

The contact line is the line of intersection between the trapped interior liquid–liquid interface and liquid–gas free-surface at $x=x_*(t)$. These layers meet as at an angle θ_d, the contact angle, measured through the liquid. From the moment of initial contact through to the formation of a smooth free-surface, θ_d evolves from 180° to 90°. By the conditions of continuity of surface flux and acting forces on the contact line

$$(\varrho\mathbf{w})_1\cdot\mathbf{e}_1+(\varrho\mathbf{w})_2\cdot\mathbf{e}_2=0 \tag{11}$$

and

$$\sigma_1 \cos\theta_d + \sigma_2 = 0. \tag{12}$$

The subscripts 1 and 2 denote the limits of a function as the position vector **r** tends to the contact line along the free-surface and along the trapped interior liquid–liquid layer respectively. The unit vectors $\mathbf{e}_1$ and $\mathbf{e}_2$ are directed along these interfaces, and point away from the contact line.

If $\tau = 0$ in (3)–(9), then these equations become equal to the boundary conditions in the classical continuum formulation for viscous free-surface flow.

3. Coalescing cylinders and spheres

We now solve this model for two cases: both involve two coalescing fluid volumes of equal radii, of the same viscous liquid, coalescing in a vacuum or in an inviscid gas. In the first case these volumes are cylinders, and in the second case spheres. The impact speeds U_∞ of the coalescing volumes, in both cases, are taken to be equal and sufficiently small to ensure that the early stages of coalescence are self-similar. We solve here for small times when the contact angle $\theta_d \approx 180°$. We examine small time asymptotics so that $t \ll \tau$ where $t = 0$ is the moment of impact. We also assume that the distance of the contact line from the impact point $x_*(t)$ is much less than the droplet radius R for small times much less than τ.

The origin is located at the impact point, and for the coalescence of two cylinders, the Cartesian (x, y) coordinate system is used where the x-axis points through the cusp between the cylinders and the y-axis lies on the centre of each cylinder, so that the x-axis is between the two cylinders at the moment of impact. Cylindrical coordinates are used instead for two coalescing spheres, and here the x-coordinate becomes a radius from the central axis of the cylindrical polar system and the y-coordinate is the distance along this central axis, again through the centre of each sphere (Fig. 2). The trapped internal liquid–liquid interface is then at $y = 0$ for $0 < x < x_*(t)$. (By symmetry, it will only be necessary to solve the equations for $y \geqslant 0$ and $x \geqslant 0$.) The contact line at the opening propagating cusp is at $x = x_*(t)$, $y = 0$.

The following similarity transformation is used to solve Eqs. (1) and (2) subject to boundary conditions (3) to (9), (11) and (12):

$$\xi = \frac{x}{\sqrt{t}} \quad \text{and} \quad \eta = \frac{y}{\sqrt{t}}. \tag{13}$$

The equations are non-dimensionalised using the scales for time, length, velocity, pressure, surface tension and surface density

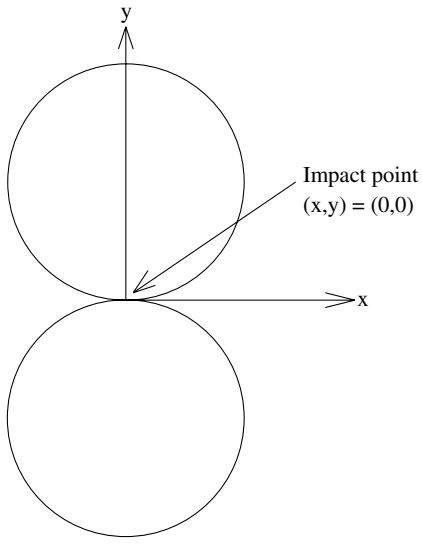

Fig. 2. Coordinate system used for the small time asymptotics.

$$\tau, \quad L = (\tau\nu)^{\frac{1}{2}}, \quad U_0 = \left(\frac{\nu}{\tau}\right)^{\frac{1}{2}}, \quad \frac{\mu}{\tau}, \quad \sigma_{1e}, \quad \varrho_0, \tag{14}$$

respectively and all quantities will from now be taken to be non-dimensional.

On the x-axis, for $0 \leqslant x \leqslant x_*(t)$, behind the cusp, particles are gradually loosing their surface properties and this path traced behind the opening, propagating cusp is the surface tension relaxation tail. The length scale L is the characteristic length associated with the surface tension relaxation tail, and U_0 is the characteristic velocity associated with the surface tension flow which is assumed to be dominant over the impact speed U_∞ of the drops. Under this non-dimensionalisation the Reynolds number becomes unity. The self-similar location of the cusp is given by

$$x_*(t) = \xi_* t^{\frac{1}{2}} \tag{15}$$

and the asymptotic limit

$$\frac{U_\infty}{U_0} \to 0, \quad \frac{R}{L} \to \infty, \quad \frac{U_\infty}{U_0}\frac{R}{L} \equiv \frac{U_\infty R}{\nu} = \frac{\xi_*^2}{2} = \text{constant}, \quad K_1 = \frac{\delta l}{L} \to 0, \tag{16}$$

is assumed, allowing for slow impact coalescence of large droplets. With $K_1 \ll 1$, we have that the thickness of the interfacial layer δl is much less than the typical length of the surface tension relaxation tail L.

In Blake and Shikhmurzaev (2002) it was estimated that $\tau \propto \mu$. The lowest estimates for τ in Blake et al. (1999) and Blake and Shikhmurzaev (2002) (for low viscosity liquids such as water) are of the order 10^{-9} s. If this is so, then one might also expect highly viscous silicone oils to have τ of the order 10^{-3} s. Therefore, the characteristic length associated with the surface tension relaxation tail, L in (14), can be expected to vary from 10^{-8} m to 10^{-2} m. In *I*, it was estimated that δl is of the order nanometres for simple fluids. Taking this, one can estimate that K_1 will range from 0.1 (for low viscosity liquids) to 10^{-7} (for highly viscous liquids). However, much more work needs to be done on experimental estimates for τ, for which there is some disagreement.

The small time, self-similar asymptotic expansions used for bulk velocity, pressure, surface density and surface velocity are

$$\begin{aligned}
&u(x,y,t) = tU(\xi,\eta) + o(t),\\
&v(x,y,t) = V_0(\xi,\eta) + tV(\xi,\eta) + o(t),\\
&p(x,y,t) - p_0 = \sqrt{t}P(\xi,\eta) + o(\sqrt{t}),\\
&\varrho(x,t) = \bar{\varrho}_{1e} + tF_i(\xi) + o(t),\\
&u_s(x,t) = \sqrt{t}S_i(\xi) + o(\sqrt{t}),\\
&v_s(x,t) = tV^s(\xi) + o(t)\\
&(i = 1,\ \xi > \xi_*;\ i = 2,\ 0 \leqslant \xi < \xi_*)
\end{aligned} \tag{17}$$

as $t \to 0$, where $\mathbf{u} = u\mathbf{e}_x + v\mathbf{e}_y$, $\mathbf{w} = u_s\mathbf{e}_x + v_s\mathbf{e}_y$, p is the non-dimensional fluid pressure and p_0 the non-dimensional pressure in the gas that is adjacent to the liquid free-surface. The expansion for $\varrho(x, t)$ means that the surface tension at $t = 0$ on the liquid–liquid internal interface is equal to the free-surface equilibrium value. Here U and V are the self-similar bulk velocity components and P the transformed pressure. The subscript i in Eq. (17) is set to '2' for values that apply on the trapped interior liquid–liquid interface, and '1' if they apply on the liquid–gas free-surface. The tangential, self-similar surface velocity component is therefore S_1 along the liquid–liquid interface and S_2 along the liquid–gas interface. The unit vectors $\mathbf{e}_x$ and $\mathbf{e}_y$ point in the directions of the positive x and y axes. It will be seen that the free-surface is mapped to $\eta = 0$, $\xi > \xi_*$ for small times.

The non-dimensional equilibrium surface density that applies to the liquid–gas interface is

$$\bar{\varrho}_{1e} = \frac{\varrho_{1e}}{\varrho_0},$$

so that in non-dimensional terms (10) becomes

$$\bar{\varrho}_e = \begin{cases} 1, & 0 \leqslant x < \xi_* t^{\frac{1}{2}}, \\ \bar{\varrho}_{1e}, & x > \xi_* t^{\frac{1}{2}} \end{cases}$$

for small times. Therefore the non-dimensional equilibrium surface density on the internal liquid–liquid interface becomes equal to one. The kinematic condition (3) on the interior liquid–liquid interface becomes

$$\mathbf{w} \cdot \mathbf{n} = 0. \tag{18}$$

Then from this and Eqs. (1), (2), (9) and (17) we find

$$V_0 = K_1(\bar{\rho}_{1e} - \bar{\rho}_e),$$

so that $V_0 = O(K_1)$, and hence negligible in this asymptotic limit. It follows from Eqs. (9), (17) and (18) that

$$V^s(\xi) = \begin{cases} 0, & 0 \leqslant \xi < \xi_*, \\ V(\xi) - K_1 F_1(\xi), & \xi > \xi_*. \end{cases} \tag{19}$$

Defining the integer variable j such that in the cylindrical case $j = 0$, and for the spherical case $j = 1$, the stream function that satisfies the continuity equation is

$$U = \left(-\frac{1}{\xi}\right)^j \frac{\partial \Psi}{\partial \eta}, \quad V = -\left(-\frac{1}{\xi}\right)^j \frac{\partial \Psi}{\partial \xi}. \tag{20}$$

It follows that the small-time asymptotic, self-similar, equation for Ψ which governs the initial stages of coalescence, is

$$\begin{aligned} &-\left\{\frac{\xi}{2}\frac{\partial^3 \Psi}{\partial \xi \partial \eta^2} + \frac{\xi}{2}\frac{\partial^3 \Psi}{\partial \xi^3} + \frac{\eta}{2}\frac{\partial^3 \Psi}{\partial \xi^2 \partial \eta} + \frac{\eta}{2}\frac{\partial^3 \Psi}{\partial \eta^3}\right\} + \frac{j}{2}\left\{3\frac{\partial^2 \Psi}{\partial \xi^2} - \frac{3}{\xi}\frac{\partial \Psi}{\partial \xi} + 2\frac{\partial^2 \Psi}{\partial \eta^2} + \frac{\eta}{\xi}\frac{\partial^2 \Psi}{\partial \xi \partial \eta}\right\} \\ &\quad = \frac{\partial^4 \Psi}{\partial \xi^4} + 2\frac{\partial^4 \Psi}{\partial \xi^2 \partial \eta^2} + \frac{\partial^4 \Psi}{\partial \eta^4} + j\left\{\frac{3}{\xi^2}\frac{\partial^2 \Psi}{\partial \xi^2} - \frac{3}{\xi^3}\frac{\partial \Psi}{\partial \xi} - \frac{2}{\xi}\frac{\partial^3 \Psi}{\partial \xi^3} - \frac{2}{\xi}\frac{\partial^3 \Psi}{\partial \xi \partial \eta^2}\right\} \end{aligned} \tag{21}$$

subject to the boundary conditions

$$\Psi \to 0 \quad \text{as } \xi^2 + \eta^2 \to \infty, \tag{22}$$

$$\Psi = 0 \text{ and } \frac{\partial}{\partial \xi}\left(\frac{1}{\xi^j}\frac{\partial \Psi}{\partial \xi}\right) = 0 \quad \text{at } \xi = 0, \tag{23}$$

$$\frac{1}{\xi^j}\frac{\partial \Psi}{\partial \xi} = -K_1 F_2(\xi), \quad 0 < \xi < \xi_*, \ \eta = 0, \tag{24}$$

$$\left(-\frac{1}{\xi}\right)^j \left(\frac{\partial^2 \Psi}{\partial \eta^2} - \frac{\partial^2 \Psi}{\partial \xi^2}\right) = \frac{\lambda}{C_a}\frac{\mathrm{d}F_2}{\mathrm{d}\xi}, \quad 0 < \xi < \xi_*, \ \eta = 0, \tag{25}$$

$$\left(-\frac{1}{\xi}\right)^j \left(\frac{\partial^2 \Psi}{\partial \eta^2} - \frac{\partial^2 \Psi}{\partial \xi^2}\right) = \frac{\lambda}{C_a}\frac{\mathrm{d}F_1}{\mathrm{d}\xi} \quad \text{at } \eta = 0, \ \xi > \xi_*, \tag{26}$$

and

$$\frac{3}{\xi^j}\frac{\partial^3 \Psi}{\partial \xi^2 \partial \eta} + \left(\frac{\xi^{1-j}}{2} - \frac{3j}{\xi^2}\right)\frac{\partial^2 \Psi}{\partial \xi \partial \eta} - \left(\frac{3}{2\xi}\right)^j \frac{\partial \Psi}{\partial \eta} + \frac{1}{\xi^j}\frac{\partial^3 \Psi}{\partial \eta^3} = 0 \tag{27}$$

at $\eta = 0$, $\xi > \xi_*$. The propagating opening cusp is then at $\eta = 0$, $\xi = \xi_*$, with the free-surface on $\eta = 0$ for $\xi > \xi_*$, and with the trapped interior liquid–liquid layer on $\eta = 0$ for $0 < \xi < \xi_*$. The non-dimensional constants are

$$C_a = \left(\frac{\mu^3}{\sigma_{1e}^2 \rho \tau}\right)^{\frac{1}{2}}, \quad \lambda = \frac{\gamma \varrho_0}{\sigma_{1e}} = \frac{1}{1 - \bar{\varrho}_{1e}},$$

where C_a is the Capillary number.

Eq. (21) arises from the Navier–Stokes equation (2), and boundary condition (22) follows from the asymptotic limit of Eq. (16). Boundary conditions (23) are conditions of symmetry, which can also be written as

$$u_s = 0, \quad u \equiv 0, \quad \frac{\partial v}{\partial x} \equiv 0 \ \text{ at } x = 0, \tag{28}$$

which enables us to solve in the region $\eta \geqslant 0$ and $\xi \geqslant 0$ (or equivalently $x \geqslant 0$ and $y \geqslant 0$). Combining Eqs. (9), (17) and (18) we obtain boundary condition (24). (Note that in Eq. (24) we retain an $O(K_1)$ term, even though we use the limit $K_1 \to 0$ here. We shall do this in order to investigate the effect of K_1 small but finite in some of our numerical simulations, pushing the asymptotics strictly beyond their validity, in order to understand the role of the right-hand side of (9) in the model, neglected in *I*.) Boundary conditions (25) and (26) are derived by applying the tangential stress boundary condition, Eq. (4), along the free-surface combined with the surface equation of state (6). Substituting the surface velocity and density expansions from Eq. (17) into the surface continuity equation (7), and combining this with the surface equation of state and surface tension gradient relation, Eqs. (6) and (9) respectively, give at leading order

$$F_i'' + \left(a\xi + \frac{j}{\xi}\right)F_i' - 2aF_i = -b_i, \tag{29}$$

where a prime denotes differentiation with respect to ξ and

$$a = \frac{B}{2\lambda\bar{\varrho}_{1e}}, \quad b_1 = 0, \quad b_2 = \frac{B}{\lambda^2\bar{\varrho}_{1e}}, \quad B = \frac{4\beta v}{\sigma_{1e}(1+4\alpha\beta)}.$$

Here α and β are liquid constants, and estimates for their values (Blake and Shikhmurzaev, 2002) are $\beta = \mu/\delta l$ and $\alpha\beta = 1$. The surface density function $F_i(\xi)$, from Eq. (17), is related to the horizontal surface velocity function $S_i(\xi)$ by

$$S_i = -\frac{\lambda}{B}\frac{\mathrm{d}F_i}{\mathrm{d}\xi} \tag{30}$$

from Eqs. (6) and (8). It follows Eqs. (10)–(12) that

$$F_2'(0) = 0, \quad F_1(\xi_*) = F_2(\xi_*), \quad F_1(\infty) = 0, \quad F_1'(\xi_*) = F_2'(\xi_*). \tag{31}$$

The solution of (29) and (31) is

$$F_1 = C_1\left(2^j + a\xi^2\right)\int_\xi^\infty \frac{\exp(-a\xi^2/2)}{\xi^j\left(2^j + a\xi^2\right)^2}\mathrm{d}\xi, \tag{32}$$

$$F_2 = \frac{b_2}{2a} - C_2\left(2^j + a\xi^2\right), \tag{33}$$

where

$$C_1 = \frac{b_2\xi_*^{j+1}}{a}\exp(a\xi_*^2/2) \tag{34}$$

and

$$C_2 = \frac{b_2}{2a\left(2^j + a\xi_*^2\right)}\left\{1 - 2a\xi_*^{j+1}\exp\left(\frac{a\xi_*^2}{2}\right)\left(2^j + a\xi_*^2\right)\int_{\xi_*}^\infty \frac{\exp(-a\xi^2/2)}{\xi\left(2^j + a\xi^2\right)^2}\mathrm{d}\xi\right\}. \tag{35}$$

Eq. (3) is the kinematic boundary condition where G represents the free-surface position. In the case of the coalescing cylinders or spheres,

$$G(x, y, t) = y - f(x, t) = 0. \tag{36}$$

We pose the expansion

$$f = tf_1(\xi) + t^2 f_2(\xi) + O(t^3) \tag{37}$$

for the position of the free-surface where f is non-dimensional. Substituting this expansion for f from Eq. (37), along with the self-similar expansions for u_s and v_s from Eq. (17), into Eq. (3), and combining with Eqs. (9) and (13), the kinematic boundary condition becomes

$$-f_1(\xi)+\frac{1}{2}\xi\frac{\partial f_1}{\partial \xi}=0 \tag{38}$$

at O(1), while at O(t) we get

$$-2f_2+\frac{1}{2}\xi\frac{\partial f_2}{\partial \xi}-S_1\frac{\partial f_1}{\partial \xi}+V(\xi,0)-K_1F_1(\xi)=0. \tag{39}$$

The above equations are valid on the free-surface (i.e. for $\xi>\xi_*$). Eq. (38) has the solution

$$f_1(\xi)=A\xi^2, \tag{40}$$

where A is a constant of integration. Using the above solution and Eq. (30), Eq. (39) gives

$$f_2(\xi)=-2\xi^4\int_{\xi_*}^{\xi}\left(\frac{V(\beta,\eta=0)+K_2\beta F_1'(\beta)-K_1F_1(\beta)}{\beta^5}\right)\mathrm{d}\beta, \tag{41}$$

where

$$K_2=\frac{2A\lambda}{B}.$$

At the cusp, i.e. $\xi=\xi_*$, f_2 is zero because $y=f=0$ here. The integral in (41) converges because as $\xi\to\infty$, $V\to 0$ and $F_1'\to 0$. Eq. (41) corresponds to the correction to the position of the free-surface in response to the flow generated by the surface tension relaxation process. The term f_1 corresponds to the initial shape of the free-surface before impact. This can be seen since $f_1=A\xi^2=Ax^2/t$, so that at leading-order in t, $f=Ax^2$. The initial shape of the free-surface is $f=(R\pm\sqrt{R^2-x^2L^2})/L$ (in non-dimensional notation) since it is initially cylindrical or spherical at the moment before impact. Hence from (16),

$$f=\frac{L}{2R}x^2+\mathrm{O}\left(\frac{L^3}{R^3}\right) \tag{42}$$

at the moment of impact at $t=0$ (taking the negative alternative root since this corresponds to the free-surface position close to the impact point). Therefore, $A=L/(2R)$ which gives that $A\to 0$ in the limit $L/R\to 0$, from Eq. (16) used here. Hence $K_2\to 0$ in (41). Also, $K_1\to 0$ in (41) from (16).

Finally we note that substituting the expansion for f given by Eq. (37), along with the asymptotic expansions for u, v and p from (17), into Eq. (5), the normal stress boundary condition, gives

$$P=2\frac{\partial V}{\partial \eta} \tag{43}$$

on $\eta=0$ (on the free-surface). Therefore, boundary condition (43) should be applied on the liquid–gas interface, $\eta=0$, $\xi>\xi_*$. Boundary condition (27) corresponds to the stream function formulation of Eq. (43). Therefore, the normal stress boundary condition (27) and (43) means that the flow induced by the surface tension relaxation process causes a correction in small times to the position of the free-surface, given by Eq. (41). That is, we find that the surface tension relaxation process causes the liquid–gas free-surface to move with time.

4. Local asymptotics close to the propagating opening cusp

One can carry out an analysis of the flow in the vicinity of the propagating opening cusp by deriving a local asymptotic approximation. The cylindrical case is considered in this section only for simplicity. The following expansion is posed for the stream function close to the opening propagating cusp

$$\Psi=\Psi_*+r\hat{f}(\theta)+r^2\hat{g}(\theta)+r^3\ln(r)\hat{h}(\theta)+r^3\hat{l}(\theta)+r^4\ln(r)\hat{m}(\theta)+r^4\hat{n}(\theta)+\mathrm{O}(r^5), \tag{44}$$

where

$$r = (\xi - \xi_*)^2 + \eta^2, \quad \tan(\theta) = \frac{\eta}{\xi - \xi_*}$$

valid for $r \to 0$. Substituting the expansion given by Eq. (44) into Eq. (21) (for $j = 0$ for cylinders), subject to boundary conditions (24)–(27), gives

$$\Psi_* = K_1 F_2(\xi_*), \tag{45}$$

$$\hat{f}(\theta) = D_1 \sin(\theta) - \frac{K_1 C_a \alpha_0}{\lambda} \cos(\theta), \tag{46}$$

$$\hat{g}(\theta) = \frac{\sin(\theta)}{2}\{\alpha_1 \sin(\theta) + 4D_3 \cos(\theta)\} - \frac{K_1 C_a \alpha_1}{2\lambda}, \tag{47}$$

$$\hat{h} = \frac{\sin(\theta)}{4\pi}(\alpha_2 + \beta_2)\big(2\cos^2(\theta) - 1\big), \tag{48}$$

$$\begin{aligned}\hat{l}(\theta) = {} & \frac{1}{12} D_1 \sin(\theta)(4\cos^2(\theta) - 1) + 2D_2 \sin(\theta)(1 - 4\cos^2(\theta)) \\ & - \alpha_2 \frac{\theta}{2\pi} \cos(\theta)\sin^2(\theta) + \frac{1}{2}\beta_2 \sin^2(\theta)\cos(\theta)\left(1 - \frac{\theta}{2\pi}\right) \\ & + \frac{1}{12} D_3 \xi_* \sin(\theta)\big\{1 + 4\cos^2(\theta)\big\} + \frac{K_1 C_a \alpha_2 \cos(\theta)}{6\lambda}\big\{3 - 2\cos^2(\theta)\big\},\end{aligned} \tag{49}$$

$$\hat{m}(\theta) = -\frac{1}{96\pi} \sin(\theta)\cos(\theta)[(\alpha_2 + \beta_2)\xi_* + 16(\alpha_3 + \beta_3)(4\cos^2(\theta) - 3)] \tag{50}$$

and

$$\begin{aligned}\hat{n}(\theta) = {} & \frac{D_3}{96} \sin(\theta)\cos(\theta)\{\xi_*^2 + 4\} + 2D_4 \sin(\theta)\cos(\theta)\{4\cos^2(\theta) - 3\} \\ & - \frac{D_1 \xi_*}{96} \sin(\theta)\cos(\theta) + \frac{D_2 \xi_*}{12} \sin(\theta)\cos(\theta) - \frac{\alpha_2 \xi_*}{2304\pi}\{24\cos^2(\theta)[\theta + 3\pi] - 6[5\theta + 3\pi] \\ & - 48\cos^4(\theta) + 7\sin(\theta)\cos(\theta)\} - \frac{\beta_2 \xi_*}{2304\pi}\{30[\pi - \theta] + 24\cos^2(\theta)[\theta - \pi] + 7\sin(\theta)\cos(\theta)\} \\ & - \frac{\alpha_3 \theta}{6\pi}\{1 - 5\cos^2(\theta) + 4\cos^4(\theta)\} + \frac{\beta_3}{6\pi}\{\theta - \pi + 5\cos^2(\theta)[\pi - \theta] + 4\cos^4(\theta)[\theta - \pi]\} \\ & + \frac{K_1 C_a \alpha_3}{12\lambda}\{3 - 12\cos^2(\theta) + 8\cos^4(\theta)\} + \frac{K_1 C_a \xi_* \alpha_2}{24\lambda}\{2\cos^2(\theta) - 1 - \cos^4(\theta)\},\end{aligned} \tag{51}$$

where

$$\alpha_0 = \frac{\lambda}{C_a} F_2(\xi = \xi_*), \quad \alpha_1 = \beta_1 = \frac{\lambda}{C_a}\frac{\mathrm{d}F_2}{\mathrm{d}\xi}(\xi = \xi_*), \quad \alpha_2 = -\frac{\lambda}{C_a}\frac{\mathrm{d}^2 F_2}{\mathrm{d}\xi^2}(\xi = \xi_*),$$

$$\beta_2 = \frac{\lambda}{C_a}\frac{\mathrm{d}^2 F_1}{\mathrm{d}\xi^2}(\xi = \xi_*), \quad \alpha_3 = 0, \quad \beta_3 = \frac{\lambda}{2C_a}\frac{\mathrm{d}^3 F_1}{\mathrm{d}\xi^3}(\xi = \xi_*),$$

and D_1, D_2, D_3 and D_4 are undetermined constants. (Again, we note that $K_1 \to 0$ in our asymptotic limits chosen in this paper (16), but once again we retain these terms here so that we have an opportunity to estimate their effect in our simulations, pushing the asymptotics strictly beyond their validity, for illustrative purposes.) We do not expect to get a closed solution free of unknown constants in this local asymptotic expansion since the partial differential equation is elliptic. It follows from Eqs. (20), (44) and (51) that

$$D_1 = U(\xi = \xi_*, \eta = 0). \tag{52}$$

An asymptotic approximation, on the liquid–gas interface adjacent to the cusp, for the leading-order vertical surface velocity component and the free-surface function f_2 from Eq. (41), can be found by combining Eqs. (17), (19), (20), (40), (41), and (44)–(51), and after some algebra we find

$$V^s(\xi_* + r) = -\frac{K_1 b_2}{2} r^2 + \mathrm{O}(r^3) \tag{53}$$

and

$$f_2(\xi_* + r) = \frac{8\lambda a \xi_* A C_2}{B} r + \frac{2\lambda A}{B}(aC_2 - b_2) r^2 + \frac{1}{\xi_*}\left(\frac{K_1 b_2}{3} + \frac{8A}{3B}[6\lambda a C_2 - b_2]\right) r^3 + \mathrm{O}(r^4) \tag{54}$$

as $r \to 0$ (with $r > 0$). Now K_1 (though asymptotically small) is positive, therefore Eq. (53) implies that the vertical free-surface interface velocity, immediately to the right of the cusp, is directed downwards, as the leading-order term is negative. Hence the free-surface is being zipped together as the cusp propagates away from the impact point, and so the droplets are coalescing.

As stated previously, the parameter A is asymptotically small because of an assumption here that the characteristic surface tension relaxation length is much less than the radius of the droplet. However, we can take A to be small but finite, strictly pushing the asymptotics beyond their range of applicability, but providing extra insight into the coalescence process predicted by this model. Then Eq. (54) gives

$$\frac{\mathrm{d}f_2}{\mathrm{d}\xi}(\xi = \xi_*) = \frac{8\lambda a \xi_* A C_2}{B} \tag{55}$$

as $r \to 0$, which can be used to find the correction to the contact angle θ_d for small time. If $A = 0$, the slope of f_2 at the cusp is zero. Therefore, θ_d decreases from 180° at small times only because of the effect of the geometry in the far-field, given by A.

5. Computational solution

The computational solution of the stream function equations is described here, solving Eq. (21) subject to boundary conditions (22)–(27). The numerical solution technique used is the finite difference method, and because the partial differential equation is linear and elliptic the solution of a large system of linear equations is required and is accomplished by the linear-algebra package MATLAB (2000). The finite difference scheme is second order accurate. The grid is rectangular and the grid points are equally spaced in both directions. The boundary conditions whose highest derivatives are first or second order, Eqs. (23)–(26), are applied by defining an additional line of 'ghost-points' at $\xi = -\Delta h$ or $\eta = -\Delta h$ as appropriate (where Δh is the spatial step-size). The normal stress boundary condition, Eq. (27), requires two lines of ghost-points to be defined adjacent to the liquid–gas interface (at $\eta = -\Delta h$ and $\eta = -2\Delta h$) because it contains third order derivatives. For the cylindrical cases the grid is found to converge with a mesh density of 50 spatial elements per cusp length, and the length of each side of the overall grid is equal to 8 cusp lengths. For spherical drops we have 56 spatial elements per cusp length, and the length of the sides of the grid are equal to 7 cusp lengths.

This study has not been confined to any specific type of liquid here and we vary the values of the fluid parameters to test certain aspects of the interface theory. Table 1 is a summary of the values of the model's parameters presented here. The asymptotic limit (16) has $K_1 \to 0$, so that the thickness of the interfacial layer

Table 1
Liquid parameter values used in the numerical computations

Case:	1	2	3	4
Drop shape:	Cylinder	Cylinder	Sphere	Sphere
K_1	0.00	0.11	0.00	0.00
μ (Pa s)	0.65	10^{-2}	0.65	1.5×10^{-3}
β (Pa s m^{-1})	10^5	10^4	10^5	1.5×10^6
τ (s)	10^{-3}	10^{-5}	10^{-3}	5.6×10^{-9}
ρ (kg m^{-3})	1.3×10^3	1.2×10^3	1.3×10^3	10^3
σ_{1e} (N m^{-1})	1.00	6.60×10^{-2}	1.00	6.97×10^{-2}
$\bar{\varrho}_{1e}$	0.50	0.50	0.50	0.63
ξ_*	1.00	0.69	1.00	1.41
A	0.00	0.00	3.5×10^{-2}	0.00

δl is much smaller than any other length scale in the problem. Thus we choose $K_1 = 0$ in some of our numerical computations (cases 1, 3 and 4 in Table 1). However, it is instructive to use an unphysically large value of K_1 in some computations, in order to assess the effects of this mass transfer between the bulk and the interfaces, by overestimating it (this is seen in case 2 in Table 1 where we choose $K_1 = 0.11$). When we run our computations for $K_1 \ll 1$ (e.g. $K_1 = 10^{-6}$) we cannot detect any observable differences in the results presented here when compared to running computations for $K_1 = 0$. (See Shaw, 2003 for a more comprehensive parametric study involving computations with various values for K_1 which are small but finite, and also a wide variety of other numerical solutions. However, the cases presented here capture the possibilities well.)

A highly viscous fluid is used for cases 1 and 3. It has been estimated, from experimental observations (I and Blake and Shikhmurzaev, 2002), that the surface tension relaxation time τ might be proportional to the viscosity μ and $\beta \approx \mu/\delta l$. However, if the surface tension relaxation time is large then β might be considerably less than $\mu/\delta l$ (Blake and Shikhmurzaev, 2002). For cases 2 and 4, the viscosity μ is smaller.

The stream function contour plot for case 1 is illustrated in Fig. 3 where the flow forms an anticlockwise rolling motion. On this diagram, the liquid–gas free-surface is at $\eta = 0$, $\xi > \xi_*$, while the trapped interior liquid–liquid layer is at $\eta = 0$, $0 < \xi < \xi_*$. The flow is split into two parts by a dividing streamline: inside this streamline there is an enclosed circulation flow, while the exterior streamlines flow out of the free-surface in the far-field and flow around the enclosed circulation zone. These streamlines which enter or leave the line $\eta = 0$ for $\xi > \xi_*$ correspond to a flow which moves the free-surface. Immediately to the right of the opening propagating cusp at $\eta = 0$, $\xi = \xi_*$, this flow "zips together" the free-surface ahead of the propagating, opening cusp, since the streamlines point down on this line here, and cause coalescence. These streamlines become highly compressed adjacent to the liquid–liquid interface and move adjacent to this line at $\eta = 0$, $0 < \xi < \xi_*$. Streamlines external to the dividing streamline meet up with the free-surface on the liquid–gas interface to the right of the cusp as shown in Fig. 4 which is a close-up view of Fig. 3 near the moving contact line. There is a stagnation point at the origin—the point of initial impact. The principal feature of the interface theory is the removal of the pressure singularity at the origin and this is confirmed in the pressure contour plot shown in Fig. 5 where the pressure is finite throughout the whole domain. A comparison between the

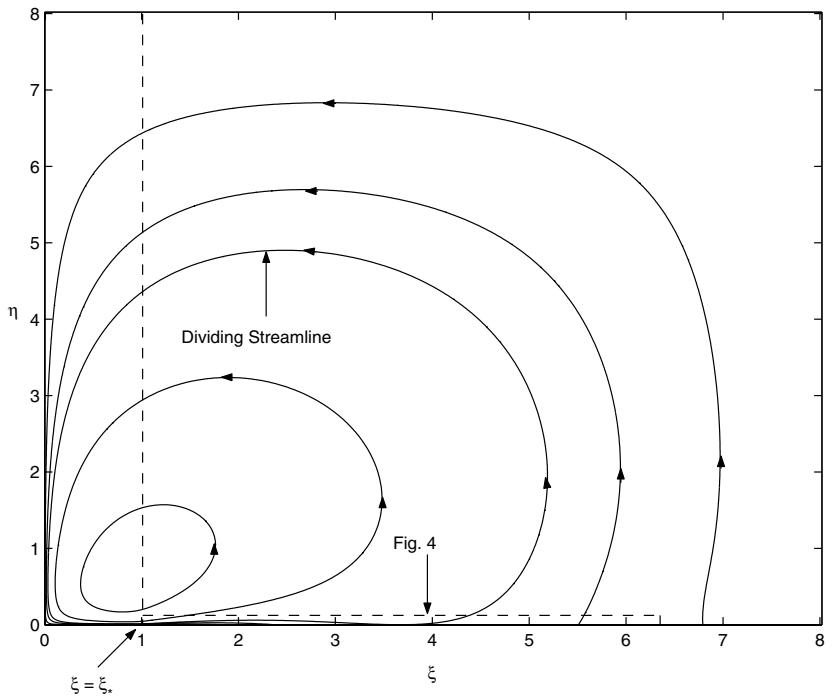

Fig. 3. Streamlines for case 1.

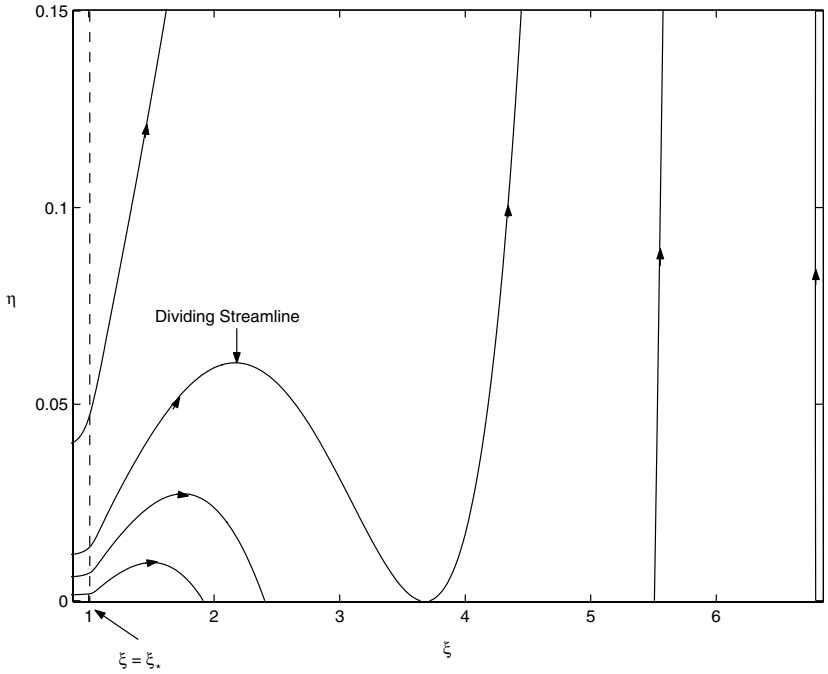

Fig. 4. Close up view of case 1, close to $\xi = \xi_*$, $\eta = 0$.

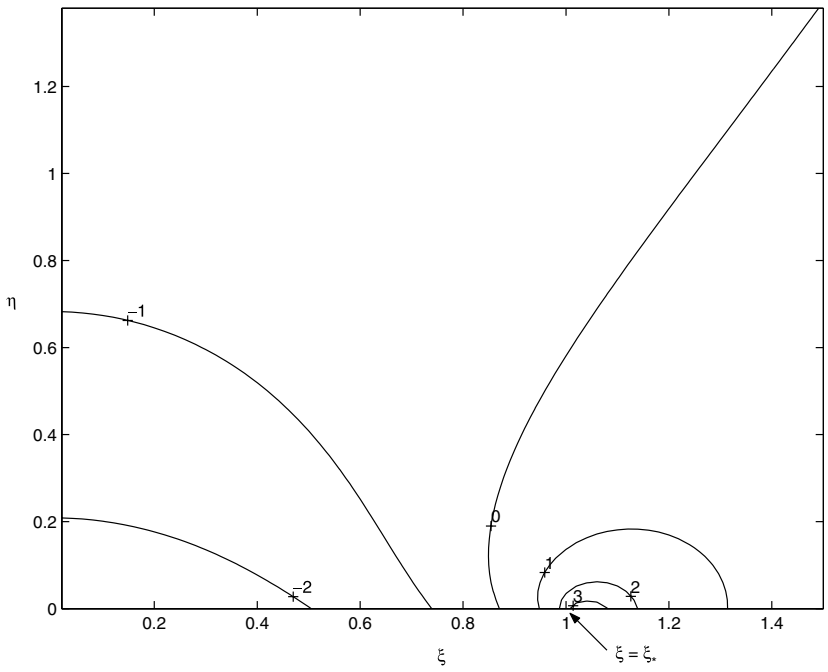

Fig. 5. Pressure contours for case 1.

numerical solution and the $r \to 0$ (near cusp) asymptotics for Ψ, calculated from Eq. (44), is shown in Fig. 6. This is a plot of Ψ along the radial line centred on the cusp and drawn at an angle $\theta = \pi/2$ radians. The two

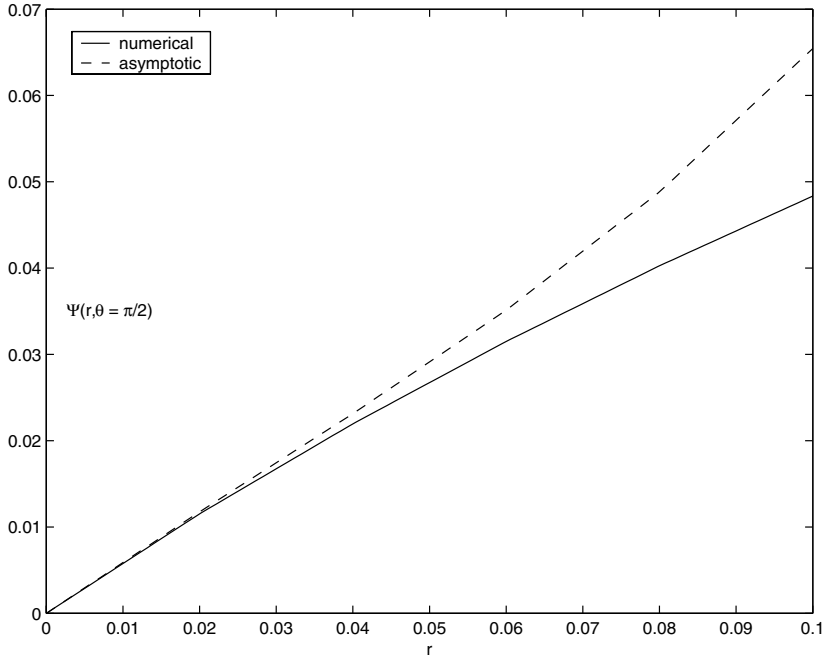

Fig. 6. Near cusp asymptotics for case 1 for $\psi(r, \theta = \pi/2)$.

curves converge as $r \to 0$. The asymptotic solution is calculated from Eq. (52) with $D_1 = 0.61$, and all the other constants D_2, D_3, and D_4 were assumed to be zero for simplicity. (Hence these higher-order coefficients do not greatly offset the near-cusp asymptotics.) This can be done for any other value of θ with similar agreement (see Shaw, 2003).

The corresponding flow for the spherical (case 3) is shown in Fig. 7—an anticlockwise rolling motion as for the above cylindrical case. Again there is an enclosed and exterior flow. There are, however, some differences observed in the flow in the vicinity of the cusp, seen in Figs. 8 and 9. (It is possible to see the lengthscale of the finite difference grid in Fig. 9, because of the very small zoomed in nature of this diagram.) From Figs. 7–9, we see that the vertical velocity component on the free-surface ($\eta = 0$, $\xi > \xi_*$) changes from negative to positive to negative and to positive again as ξ increases from ξ_*. There is again a stagnation point at the origin. Immediately to the right of the cusp at $\xi = \xi_*$ (Fig. 9) streamlines are striking the liquid–gas interface downwards, indicating that the free-surface there is closing. So again the surface tension driven flow causes the free-surface to be zipped together as the cusp propagates from left-to-right. The pressure contour plot for case 3 is illustrated in Fig. 10 and once again this shows a finite pressure everywhere.

In both the cylindrical and spherical cases, the flow is generated by surface tension which is moving the cusp away from the initial impact point. Surface tension is driving interior liquid–liquid interface particles (along this surface) towards the cusp (since S_i is positive) and this $O(t^{\frac{1}{2}})$ motion is in turn propelling an $O(t)$ anticlockwise rolling motion inside the bulk. The liquid–gas free-surface has a non-zero velocity. Streamlines are flowing into the liquid–gas interface adjacent to the cusp and hence closing up the free-surface there, as mentioned above; this is the onset of coalescence. Further away from the cusp the free-surface has an upward velocity—this is the start of the evolution of the free-surface. The differences between the cylindrical and spherical flow scenarios are geometrical: in the case of the coalescing cylinders the interior interface is an enlarging semi-infinite strip, while in the case of the spheres this will be a enlarging circular disc.

For the cases where K_1 is no longer very small a new flow layer is visible, as a result of boundary condition (24), adjacent to the trapped interior liquid–liquid interface and the liquid–gas interface immediately to the right of the cusp. The streamlines for case 2, where $K_1 = 0.11$, are plotted in Fig. 11. A close up of this new flow layer is shown in Fig. 12. There are still regions of enclosed and exterior streamlines as before with a dividing streamline, but here the stagnation point moves away from the origin to a higher

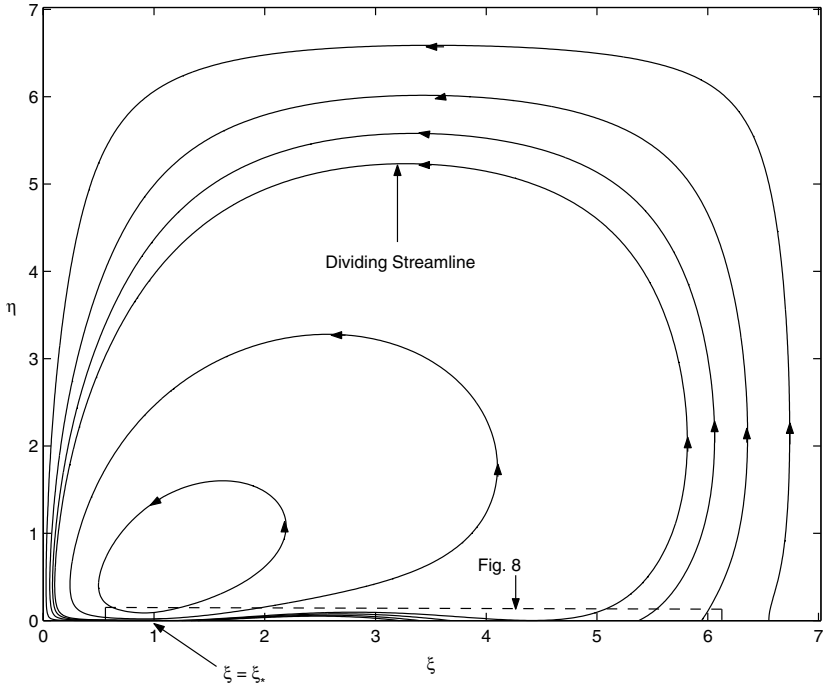

Fig. 7. Streamlines for case 3.

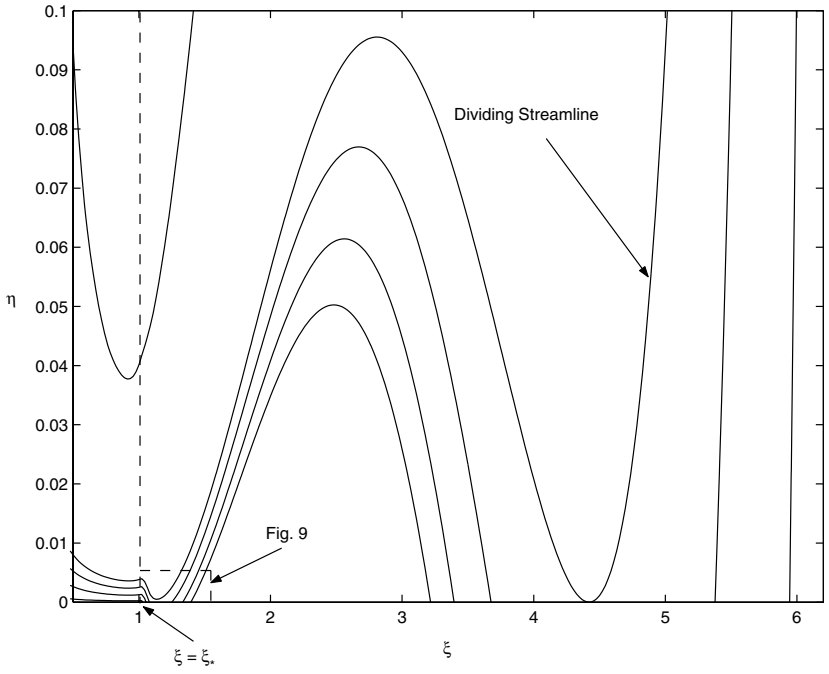

Fig. 8. Streamlines for case 3 close to $\xi = \xi_*$, $\eta = 0$.

point along the axis of symmetry (denoted SP on Fig. 12). Since K_1 is larger, a significant flow can be seen to leave the interior liquid–liquid interface at $\eta = 0$, $0 < \xi < \xi_*$ and re-enter on the liquid–gas free-surface at

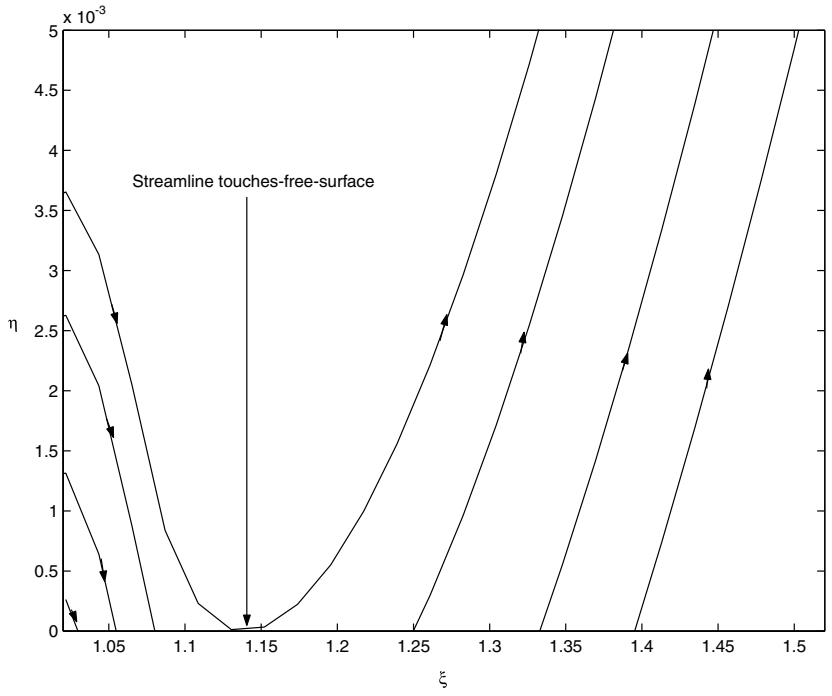

Fig. 9. Near cusp streamlines for case 3, zoomed in picture from Figs. 7 and 8.

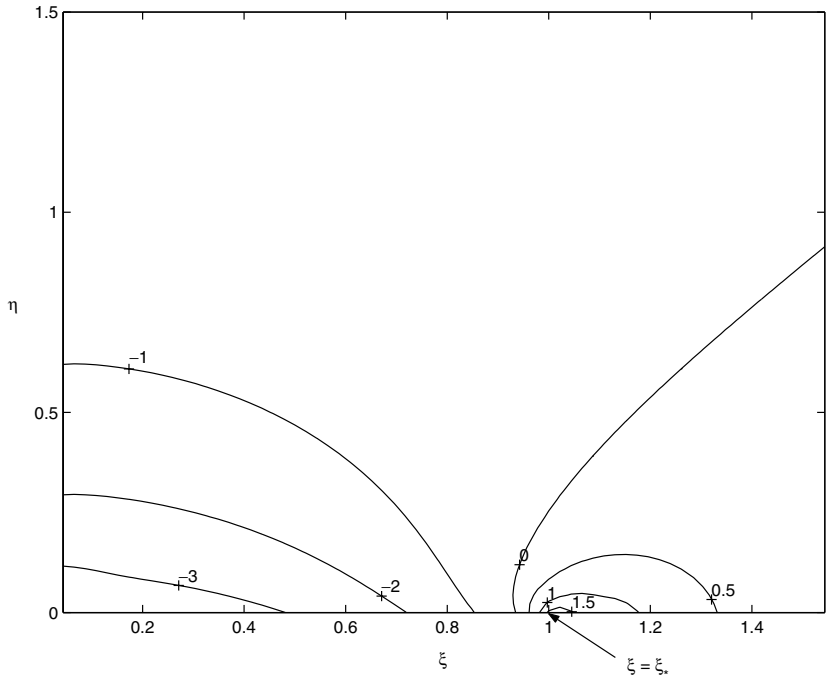

Fig. 10. Pressure contours for case 3.

$\eta = 0$, $\xi > \xi_*$. We are clearly pushing the asymptotics strictly beyond its validity by choosing $K_1 = 0.11$, and these effects are very much exaggerated. However, it is instructive to view the qualitative nature of this flow.

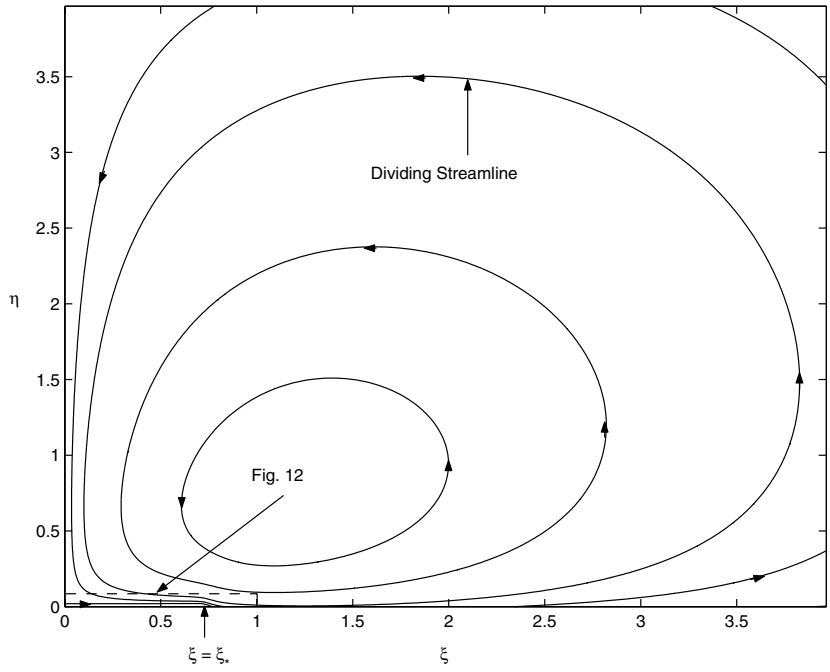

Fig. 11. Streamlines for case 2.

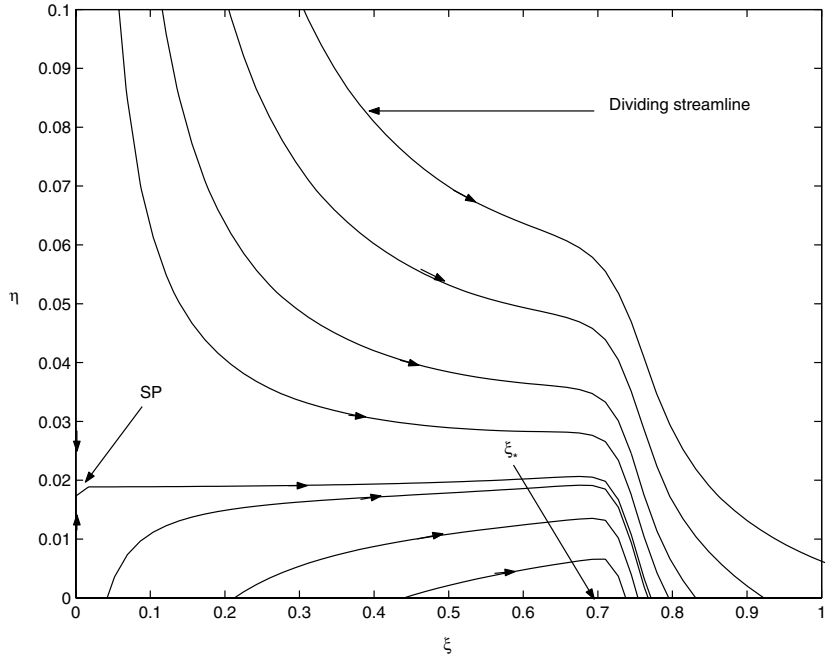

Fig. 12. Flow near liquid–liquid interface for case 2.

Streamlines for a much smaller value of τ are shown for case 4 in Fig. 13. Similarly to case 3, there are regions of interior and exterior streamlines and the flow near the cusp is similar to that shown in Figs. 8 and 9. A plot of the free-surface position for case 4, calculated from Eq. (41), is shown in Fig. 14. The slope at $\xi = \xi_*$ is zero as specified by Eq. (55) since $A = 0$ in this calculation. The constant A is asymptotically small

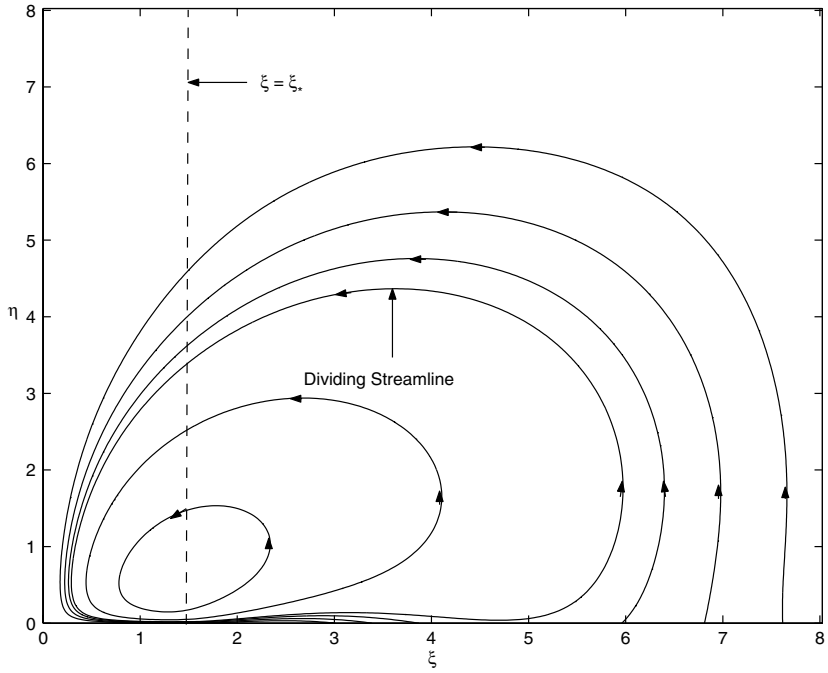

Fig. 13. Streamlines for case 4.

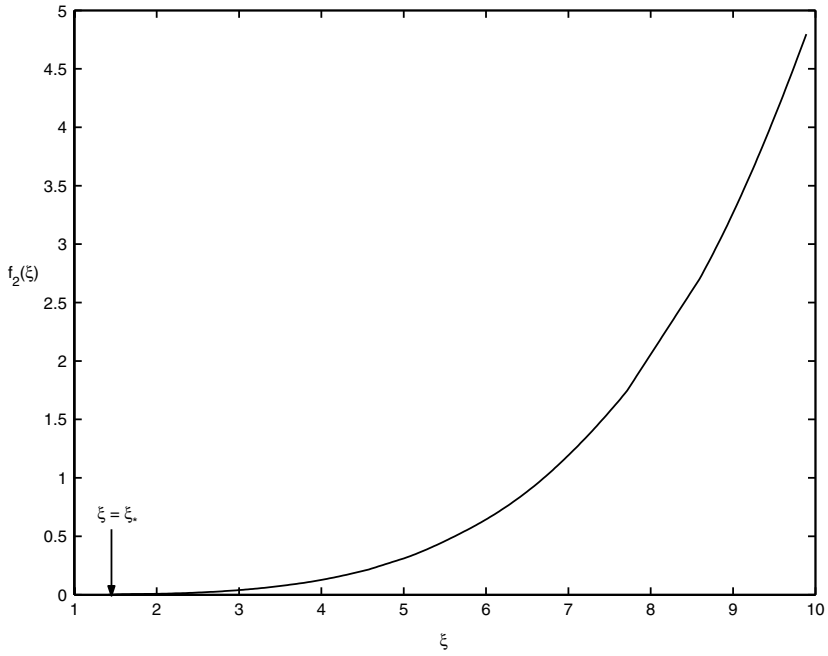

Fig. 14. Plot of $f_2(\xi)$ along the liquid–gas interface for case 4.

in this model and it is therefore not strictly correct to assign to it a non-zero value. However, a small value of A, 0.0045, is used for case 2 so that some determination can be made of the effects of the droplet impact speed and radius on the contact angle variation. A close up of f_2 in the vicinity of the cusp for case 2 is plotted in Fig. 15 and shows that the slope of f_2 at the cusp agrees with the asymptotic value calculated from Eq. (55).

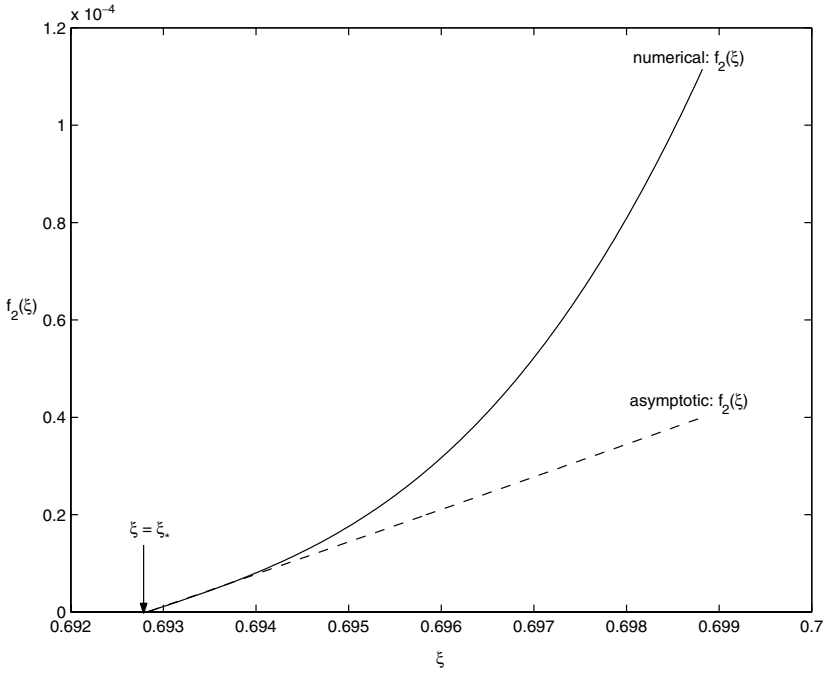

Fig. 15. Comparison of the numerical and asymptotic approximation of $f_2(\xi)$ for case 2.

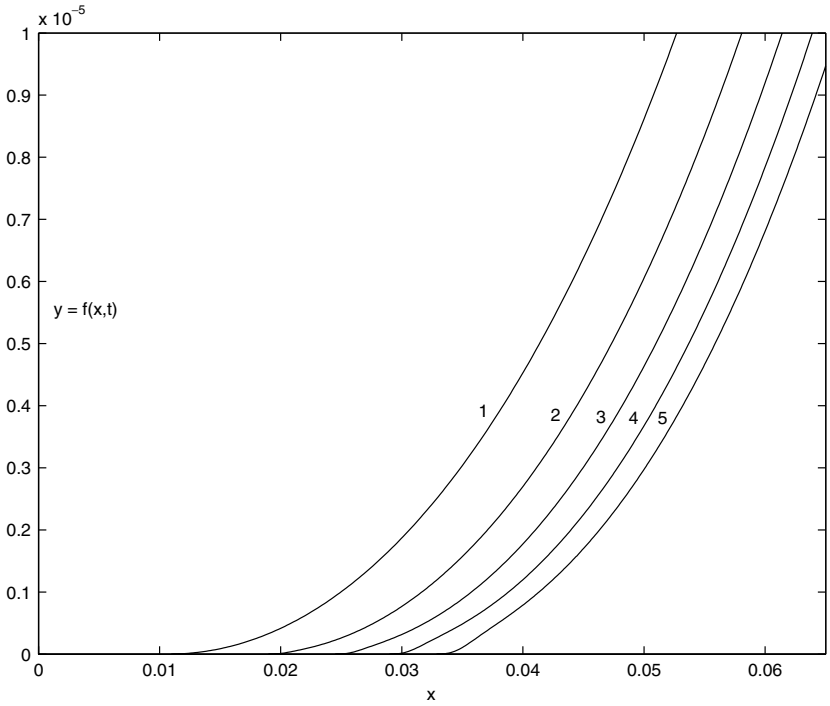

Fig. 16. Free-surface animation for case 2 at equal and increasing time intervals after the moment of impact.

Fig. 16 is a plot showing the evolution of the free-surface with time for case 2 at equal time intervals where $f(t)$ is calculated from Eq. (37). The initial slope of f at $t = 0$ is zero. Since $A > 0$ here, the slope at the opening,

Table 2
Slope at constant time intervals in free-surface animation for case 2

	Curve				
	1	2	3	4	5
t	2.5×10^{-4}	7.5×10^{-4}	1.25×10^{-3}	1.75×10^{-3}	2.25×10^{-3}
$f_2'(\xi_*)$	1.12×10^{-6}	1.16×10^{-6}	1.40×10^{-6}	1.95×10^{-6}	2.70×10^{-6}

propagating cusp increases with time because the internal contact angle decreases from 180°. Since A is small this cannot be seen easily in Fig. 16 but the slope does increase with time for each case and these values are listed in Table 2. Similar "animations" can be also produced for the $K_1 = 0$ cases, with similar results (Shaw, 2003).

Finally, note some of the qualitative features in Fig. 12 would probably also be present in Figs. 4 and 9 if instead K_1 were chosen to be very small but positive in cases 1 and 3 (as opposed to zero), but would require a very fine grid to capture them.

6. Discussion

The interface formation/disappearance theory of I has been examined at the very early stages of coalescence, immediately after impact. In I a small time, self-similar, asymptotic approximation of the model was derived for the case of two coalescing liquid cylinders which have equal volumes, and equal and opposite impact velocities that are sufficiently small for self-similarity. These asymptotics have been extended here to analyse the evolution of the free-surface at small times. Also, the equations were solved here for the first time using a finite difference method to obtain the resulting velocity and pressure fields in the flow. A small time, self-similar, asymptotic approximation of this model when applied to the case of two coalescing spheres which is more relevant to potential experiments, has also been derived and numerical solutions have been computed for that case as well. The finite difference computations have shown that the cusp propagates away from the initial impact point and the surface tension gradients result in coalescence, and confirm the removal of the pressure singularity which was inherent in the conventional approach. For the case of the coalescing cylinders, a local asymptotic approximation of the stream function in the vicinity of the cusp was derived and showed good agreement with the finite difference solution.

So far, the model has only been used to describe the very early stages of coalescence where the contact angle is close to 180°. However, to simulate the subsequent stages of coalescence it will be necessary to take into account the evolution of the contact angle and here self-similarity can no longer be assumed. Therefore it will be necessary to solve the continuity and unsteady Navier–Stokes equations (1) and (2) respectively, subject to the boundary conditions (3)–(9) with (11) and (12). In principle one could use a finite difference (e.g. Dornseifer et al., 1998), finite volume (e.g. Lafaurie et al., 1994), finite element (e.g. Gresho and Sani, 2000 and Suckling, 2003) or boundary integral method (e.g. Pergamalis, 2002 and Pozrikidis, 2002) to solve this full droplet coalescence problem. This is the subject of current work, where we have chosen the finite element method. The results of these computations will be reported at a future date. We will use this small-time solution described here as the initial condition for these simulations.

Our finite element method uses Taylor–Hood area elements to discretise the bulk spatial domain and the free-surface is approximated by quadratic line elements. The locations of the grid points are calculated using toroidal coordinates, with the advantage that it is then more straight forward to generate a mesh which is most finely refined in the vicinity of the contact line as required. Toroidal coordinates also facilitate the derivation of a hybrid Euler–Lagrange scheme that tracks the motion of the free-surface but does not tie the motion of the grid-points to the movement of continuum liquid particles. See Suckling (2003) for the initial work in this direction using finite elements.

The objective of carrying out the computations presented here was to study the liquid bridge formation, so that the correct model is identified for coalescence in important flows arising in, for example, micro-fluidics, which is an area of growing engineering importance, especially for lab-on-chip devices. Calculations here

suggest that the novel features of this flow will be most easily observed when the viscosity v is large and the impact speed U_∞ is small. The rolling motion in the liquid described here, close to the impact point, might be observable in experiments if the viscosity v is large and the droplet radius R is small. Experimental observation of these phenomena, and the liquid bridge formation in general, clearly provide a challenge to experimentalists. We hope that this, and latter works, will provide motivation for such carefully designed experiments.

References

Beysens, D.A., Andrieu, C., Nikolayev, V.S., Pomeau, Y., 2002. Coalescence of sessile drops. J. Fluid Mech. 453, 427–438.

Billingham, J., King, A.C., 2005. Surface tension driven flow outside a slender wedge with an application to the inviscid coalescence of drops. J. Fluid Mech. 533, 193–221.

Blake, T.D., Shikhmurzaev, Y.D., 2002. Dynamic wetting by liquids of different viscosity. J. Colloid Interf. Sci. 253, 196–202.

Blake, T.D., Bracke, M., Shikhmurzaev, Y.D., 1999. Experimental evidence of nonlocal hydro-dynamic influence on the dynamic contact angle. Phys. Fluids 11, 1995–2007.

Davies, J.T., Rideal, E.K., 1963. Interfacial Phenomena, second ed. Academic Press, ISBN 0-12-206056-3.

Dornseifer, T., Griebel, M., Neunhoeffer, T., 1998. Numerical Simulation in Fluid Dynamics, A Practical Introduction. Society for Industrial and Applied Mathematics, ISBN 0-89871-398-6.

Duchemin, L., Eggers, J., Josserand, C., 2003. Inviscid coalescence of drops. J. Fluid Mech. 487, 167–178.

Eggers, J., Evans, R., 2004. Comment on ''dynamic wetting by liquids of different viscosity'' by T.D. Blake and Y.D. Shikhmurzaev. J. Colloid Interf. Sci. 280, 537.

Eggers, J., Lister, J.R., Stone, H.A., 1999. Coalescence of liquid drops. J. Fluid Mech. 401, 293–310.

Gresho, P.M., Sani, R.L., 2000. Incompressible Flow and the Finite Element MethodIsothermal Laminar Flow, vol. 2. John Wiley, ISBN 0 471 49250 7.

Hopper, R.W., 1984. Coalescence of two equal cylinders—exact results for creeping viscous plane flow driven by capillarity. J. Am. Ceram. Soc. 67, C262–C264.

Hopper, R.W., 1990. Plane Stokes flow driven by capillarity on a free surface. J. Fluid Mech. 213, 349–375.

Hopper, R.W., 1992. Stokes flow of a cylinder and half-space driven by capillarity. J. Fluid Mech. 243, 171–181.

Hopper, R.W., 1993. Coalescence of two viscous cylinders by capillarity: Part II, Shape evolution. J. Am. Ceram. Soc. 76, 2953–2960.

Jeong, J.T., Moffatt, H.K., 1992. Free-surface cusps associated with flow at a low Reynolds number. J. Fluid Mech. 241, 1.

Keller, J.B., Milewski, P.A., Vanden-Broeck, J., 2000. Wetting and merging driven by surface tension. Eur. J. Mech. B-Fluids 19, 491.

Koplik, J., Banavar, J.R., 1994. Fluid cusps at the molecular scale. Phys. Fluids 6, 480–488.

Lafaurie, B., Nardone, C., Scardovelli, R., Zaleski, S., Zanetti, G., 1994. Modelling merging and fragmentation in multiphase flows with SURFER. J. Comput. Phys. 113, 134–147.

MATLAB User Manual, 2000. *Using MATLAB Version 6*. The MathWorks Inc.

Menchaca-Rocha, A., Martinez-Davalos, A., Nunez, R., Popinet, S., Zaleski, S., 2001. Coalescence of liquid drops by surface tension. Phys. Rev. E 63, 046309.

Pergamalis, H., 2002. Droplet impingement onto quiescent and moving liquid surfaces. PhD Thesis, Mechanical Engineering Department, Imperial College of Science, Technology and Medicine.

Pozrikidis, C., 2002. A Practical Guide to Boundary Element Methods with the Software Library BEMLIB. Chapman and Hall/CRC, ISBN 1584883235.

Richardson, S., 1997. Two-dimensional Stokes flows with time-dependant free-surface boundaries driven by surface tension. Eur. J.: Appl. Math. 8, 311.

Shaw, A.J., 2003. Coalescence of two liquid volumes: topological transitions in their free surface flows. MPhil Thesis, School of Mathematics and Statistics, The University of Birmingham.

Shikhmurzaev, Y.D., 1993. The moving contact line on a smooth solid surface. Int. J. Multi-phase Flow 19, 589–610.

Shikhmurzaev, Y.D., 1994. Mathematical modelling of wetting hydrodynamics. Fluid Dyn. Res. 13, 45–64.

Shikhmurzaev, Y.D., 1996. Dynamic contact angles in gas–liquid–solid systems and flow in vicinity of moving contact line. AIChE J. 42, 601.

Shikhmurzaev, Y.D., 1997. Moving contact lines in liquid/liquid/solid systems. J. Fluid Mech. 334, 211–249.

Shikhmurzaev, Y.D., 1998. On cusped interfaces. J. Fluid Mech. 359, 313–328.

Shikhmurzaev, Y.D., 2000. Coalescence and capillary breakup of liquid volumes. Phys. Fluids 12, 2386–2396.

Shikhmurzaev, Y.D., 2002. On metastable regimes of dynamic wetting. J. Phys.: Condens. Matter 14, 319–330.

Shikhmurzaev, Y.D., 2005a. Macroscopic mechanism of rupture of free liquid films. C.R. Mecanique 333, 205–210.

Shikhmurzaev, Y.D., 2005b. Fluid dynamics with transitions in the topology of the flow domain: breakup of jets and rupture of films. Doklady Phys. 50, 40–43.

Shikhmurzaev, Y.D., 2005c. Capillary breakup of liquid threads: a singularity-free solution. IMA J. Appl. Math. 70, 880–907.

Shikhmurzaev, Y.D., Blake, T.D., 2004. Response to the comment on ''dynamic wetting by liquids of different viscosity'' by J. Eggers and R. Evans. J. Colloid Interf. Sci. 280, 539–541.

Suckling, P.M., 2003. The impact and spreading of a drop on a surface. PhD Thesis, School of Mathematics and Statistics, The University of Birmingham.